BNL-100794-2015-JA

# Thermally-Induced Transition of Lamellae Orientation in Block-Copolymer Films on 'Neutral' Nanoparticle-Coated Substrates

*Kevin G. Yager,*[a] Christopher Forrey,[b] Gurpreet Singh,[c] Sushil K. Satija,[d] Kirt A. Page,[e] Derek L. Patton,[f] Jack F. Douglas,[e] Ronald L. Jones,[e] Alamgir Karim*[c]*

*a* Center for Functional Nanomaterials, Brookhaven National Laboratory, Upton NY
*b* Center for Devices and Radiological Health, Food and Drug Administration, Silver Spring, MD
*c* Department of Polymer Engineering, University of Akron, Akron, OH
*d* NIST Center for Neutron Research, National Institute of Standards and Technology, Gaithersburg, MD
*e* Polymers Division, National Institute of Standards and Technology, Gaithersburg, MD
*f* School of Polymers and High Performance Materials, University of Southern Mississippi, Hattiesburg, MS

* Corresponding Authors: kyager@bnl.gov, alamgir@uakron.edu

Note: The mention of commercial products, their sources, or their use in connection with material reported herein is not to be construed as either an actual or implied endorsement of such products by the Department of Health and Human Services.

ABSTRACT: Block-copolymer orientation in thin films is controlled by the complex balance between interfacial free energies, including the inter-block segregation strength, the surface tensions of the blocks, and the relative substrate interactions. While block-copolymer lamellae orient horizontally when there is *any* preferential affinity of one block for the substrate, we recently described how nanoparticle-roughened substrates can be used to modify substrate interactions. We demonstrate how such 'neutral' substrates can be combined with control of annealing temperature to generate vertical lamellae orientations throughout a sample, at all thicknesses. We observe an orientational transition from vertical to horizontal lamellae upon heating, as confirmed using a combination of atomic force microscopy (AFM), neutron reflectometry (NR) and rotational small-angle neutron scattering (RSANS). Using molecular dynamics (MD) simulations, we identify substrate-localized distortions to the lamellar morphology as the physical basis of the novel behavior. In particular, under strong segregation conditions, bending of horizontal lamellae induce a large energetic cost. At higher temperatures, the energetic cost of conformal deformations of lamellae over the rough substrate is reduced, returning lamellae to the typical horizontal orientation. Thus, we find that both surface interactions and temperature play a crucial role in dictating block-copolymer lamellae orientation. Our combined experimental and simulation findings suggest that controlling substrate roughness should provide a useful and robust platform for controlling block-copolymer orientation in applications of these materials.

KEYWORDS: self-assembly, orientation, nanoparticles, block copolymer, molecular dynamics, SANS.

TOC Figure/text: Using nanoparticles to tune film-substrate interactions, we demonstrate that block-copolymer lamellae undergo an orientation transition as a function of temperature.

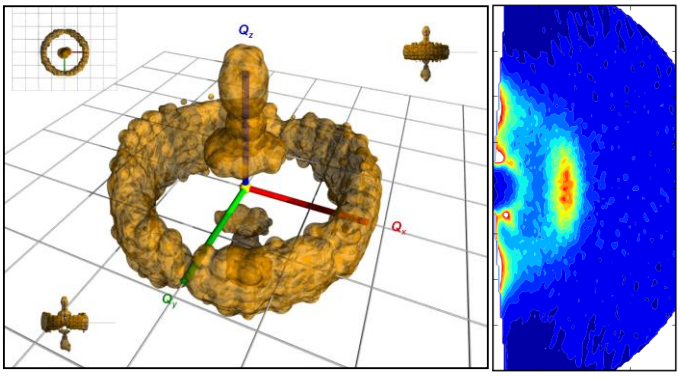

## *Introduction*

Block-copolymers (BCP) are extensively-studied self-assembling systems that phase-separate locally due to chemical incompatibility between the covalently-connected blocks. This microphase-separation can produce a variety of morphologies, with periodicities on the order of 5 nm to 100 nm.[1-4] Owing to the size-scale of the structures, these systems have been proposed as patterning layers for next-generation lithography.[5-9] The mixed chemical functionality, and tunable nanostructure, also makes these systems of interest for membranes, coatings, and many other applications.[10-11] Symmetric diblock-copolymers self-assemble into a lamellar morphology, with an intrinsic period, $L_0$, based on the block size. In thin films on flat substrates, lamellar BCPs preferentially orient with the lamellae in a horizontal arrangement: that is, parallel to the substrate interface. This occurs due to preferential wetting at both interfaces: one block will typically have an energetic preference for the substrate interface, and one block will have an energetic preference for the free surface. The horizontal orientation of the lamellae is normally stable when the total film thickness is commensurate with the lamellae period. For symmetric wetting (both the substrate and free surface are wet by the same block), the total film thickness is commensurate when it is equal to $nL_0$, where $n$ is an integer. For anti-symmetric wetting, the film is commensurate for thickness of $(n + ½)L_0$. For thin films of an incommensurate thickness, the system will relieve the instability by partitioning the free surface laterally into regions of commensurate thickness, forming so-called islands or holes.

Controlling the order and orientation of BCPs is often crucial in applications, and a variety of techniques have been developed to control order: shear alignment,[12-13] electric field alignment,[14-16] solvent annealing,[17-18] blending with copolymers,[19-22] thermal techniques (temperature gradients,[23] directional solidification,[24-25] and zone refinement,[26-32] including 'cold' zone annealing[33-36] and photo-thermal annealing[37]), topographic[38-43] and chemical patterning,[44-45] and adjusting substrate surface energy[46-49] or roughness.[50-54] The variety of available techniques emphasizes how BCP assembly is the result of a delicate balance among many competing factors. We recently demonstrated that cylinder-forming polystyrene-*block*-poly(methyl methacrylate) (PS-*b*-PMMA) BCPs exhibit a rich interfacial

morphology as a function of thickness and annealing temperature.[55] By comparison, the orientation in lamellae-forming BCPS is not normally sensitive to changes in film thickness or temperature, owing to the strong tendency of lamellar sheets to orient with substrates. However, a reorientation of lamellae into a vertically-aligned state is known to occur when the substrate[46-48, 56-57] and/or free-surface[47] lack a preferential interaction for either block; the so-called 'neutral' boundary condition. In order to understand the reorientation of lamellae-forming BCPs as a function of both thickness and temperature, it is necessary to decouple the self-assembly from its surface wetting behavior.[58] We have recently shown that one can achieve an effectively neutral substrate by roughening it with surface-adhesion of a layer of nanoparticles (NPs).[53] This surface treatment greatly reduces the strong driving force for the formation of horizontal lamellae; we previously observed that after annealing at 165 ºC, the BCP orientation was horizontal at commensurate thicknesses, but was vertical at incommensurate thicknesses. In this paper, we show that we can achieve entirely vertical lamellae orientation on these rough surfaces if we simultaneously increase the BCP segregation strength by lowering the annealing temperature. We use molecular dynamics simulations to understand the molecular basis of the combined use of interfacial interactions and temperature to achieve robust vertical ordering lamellae-forming BCP films.

## *Results*

### Morphology Diagram

In order to study the orientation of block-copolymer lamellae, we modified the film/substrate interaction by introducing roughness using our previously-described procedure.[53] These 'neutral' substrates were prepared by spin-casting solutions of propyl-coated silica nanoparticles (20 nm diameter) onto flat silicon substrates. We selected casting conditions where the root-mean-square roughness is ≈ 10 nm (supplementary information Figure S1), and oxidized the surfaces to yield an intermediate surface energy (water contact angle $\theta_w \approx 40^o$). Lammelar-forming poly(deuterated styrene)-*block*-poly(methyl methacrylate), dPS-*b*-PMMA, was spin-cast on these rough surfaces. The as-cast

block-copolymer films appear to be disordered, without any measurable phase separation or morphology development (refer to supplementary information Figures S2–S5). Microphase-separation initiated by annealing at temperatures above the glass-transition. Atomic force microscopy (AFM) images are shown for a variety of annealing temperatures, and film thicknesses, in Figure 1. The effectively flat images are indicative of horizontal lamellae (oriented parallel to substrate) whereas the 'fingerprint' patterns are indicative of vertical lamellae (perpendicular to substrate). On these rough surfaces, the vertical state appears at low annealing temperatures (≤ 150 ºC), while a horizontal state is preferred at high annealing temperatures (≥ 180 ºC). At intermediate temperatures (≈ 165 ºC), the orientation of the morphology depends on film thickness.[53] These observations can be contrasted with the normally-observed behavior of lamellae on flat non-neutral surfaces, which is to form horizontal lamellae regardless of temperature and thickness. Even a slight preferential energetic interaction between either of the blocks and the substrate will yield uniformly horizontal morphologies.

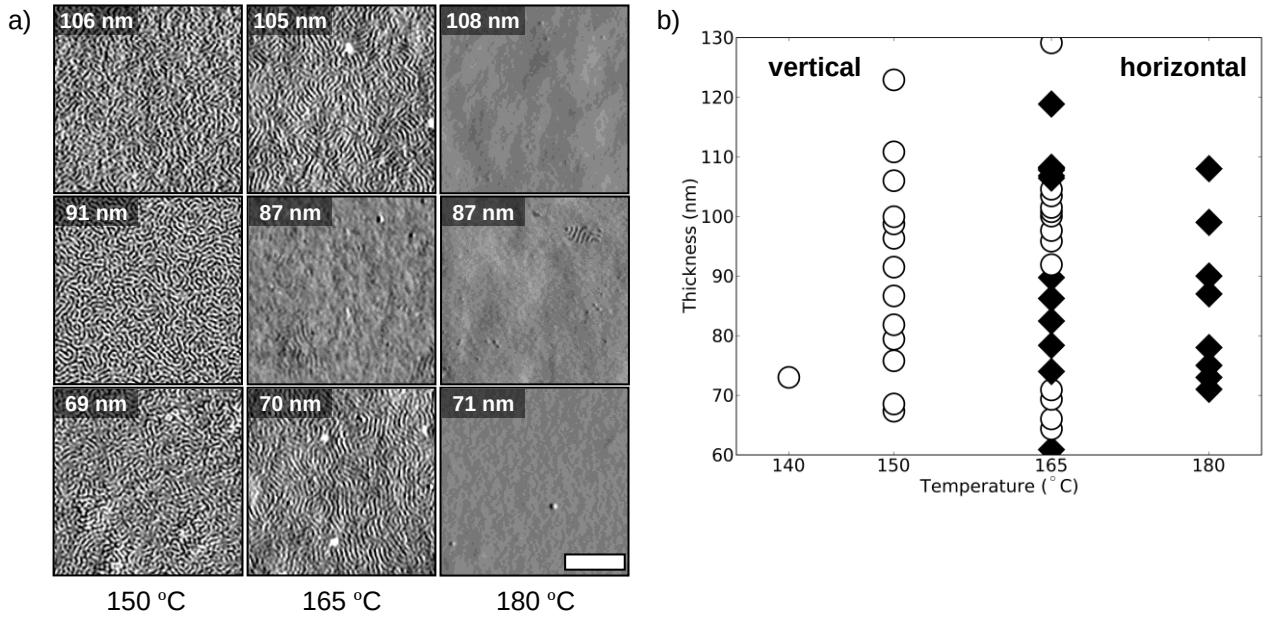


Figure 1: a) Typical AFM phase images for dPS-PMMA BCP lamellae on rough surfaces. Representative images for various thicknesses and temperatures are shown. The scale bar (lower right) is 500 nm, and applies to all images. b) Morphology orientation diagram for lamellae based on AFM image analysis. The predominantly horizontal states ($f_v$ < 25%) are denoted with black diamonds, whereas the partially or fully vertical states are denoted by open circles. There is a regime of vertical

orientation at low temperature, and a regime of horizontal orientation at higher temperature. At the boundary between the two regimes (≈ 165 ºC), a mixture of states appears, oscillating with film thickness.

The oscillation between orientations (at 165 ºC) suggests that energies of the vertical and horizontal states are nearly the same, with islands/holes tipping the energy balance one way or the other. At lower temperatures the vertical morphology evidently has a lower energy, whereas at higher temperatures the horizontal morphology is sufficiently preferred so as to compensate for the energy penalty of forming islands and holes. It is this temperature-dependent phenomenon that we seek to understand in order to control BCP lamellae orientation in thin films. We further observe that the orientation oscillation in the transition regime decays with thickness, with a horizontal surface morphology ultimately favored in arbitrarily thick samples. This is consistent with literature reports of a finite range over which the substrate directs orientation in other types of substrate-modified films.[46-47, 59] Figure 1b maps the quantification of orientation as a function of thickness and temperature. This surface-morphology diagram for BCP lamellae is analogous to that found for BCP cylinders.[55] Importantly, however, this morphology diagram only appears for lamellae when the directing effect of the substrate has been sufficiently weakened. This surface morphology diagram is apparent even after short annealing times (2 h), and remains robust for long annealing times (supplementary Figure S8), leading us to believe this is an equilibrium phenomenon.

## Lamellae Orientational Order

Although AFM is useful for quantifying the surface morphology of the ordered BCP films, it cannot address the organization of the BCPs within the film, a perennial difficulty in BCP film characterization. To probe the three-dimensional orientation of the self-assembled morphology throughout the film, we combined neutron reflectivity (NR) and small-angle neutron scattering (SANS), which are sensitive to the out-of-plane and in-plane ordering, respectively. We start by analyzing the transition region, *i.e.* at T = 165$^{o}$C, where orientation is sensitive to film thickness. Representative NR data are shown in Figure 2, where the reflectivity scans are shown alongside the corresponding best-fit for the neutron scattering-

length density (SLD) profile. Figure 2 shows three representative samples of different thicknesses. In all three cases, the SLD profile shows significant oscillations, consistent with horizontal lamellae (oriented parallel to the substrate, which is set at $z = 0$ nm in Figure 2 b): the high-SLD regions are dPS-rich (SLD of pure dPS ≈ $6.5\times10^{-6}$ Å$^{-2}$), whereas the low-SLD regions are PMMA-rich (SLD of pure PMMA ≈ $0.8\times10^{-6}$ Å$^{-2}$). The uppermost data, for a sample of total thickness 84 nm, exhibits extremely strong oscillations, indicative of well-defined horizontal lamellae throughout the entire sample. In the thinner samples, however, the SLD oscillations are not as intense. In particular, the SLD values (ranging from $1.6\times10^{-6}$ Å$^{-2}$ to $5.4\times10^{-6}$ Å$^{-2}$) indicate that only a portion of the sample adopts the horizontal orientation. In other words, these films exhibit a mixture of horizontal and vertical lamellae orientations at the top surface (confirmed by AFM, Figure 2 c). Through the film depth, we observe a preference for horizontal lamellae at the top surface, whereas there appears to be a preference for vertical lamellae closer to the substrate.

The reflectivity data for all samples indicate that the horizontal layering is strongly disrupted near the nanoparticle substrate. For samples on flat silicon (supplementary Figure S2), the oscillations in SLD persist to the substrate interface, leading to a very intense Bragg peak in the reflectivity data. However the nanoparticle-treated substrates disrupt the formation of horizontal lamellae within their vicinity. It thus appears reasonable to suggest that the vertical orientation originates at the substrate interface, whereas the horizontal state originates from the preferential wetting of dPS at the free surface.

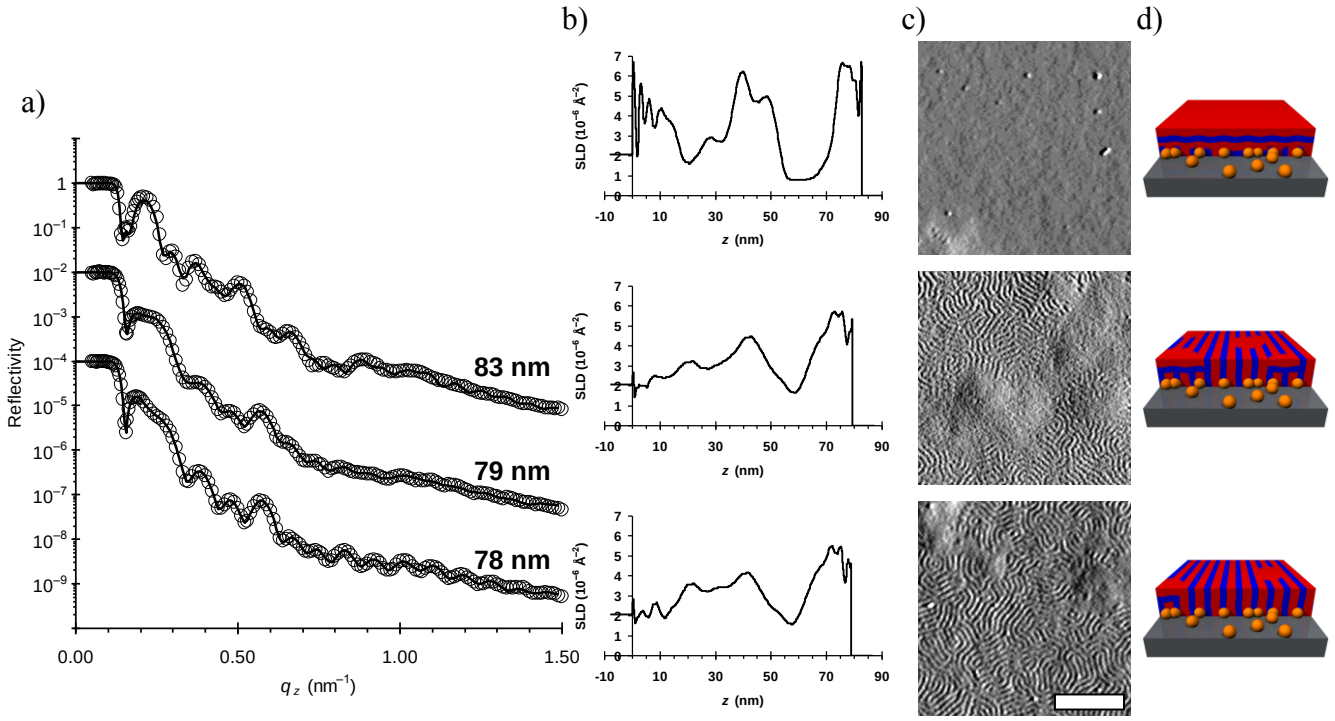


Figure 2: Neutron reflectivity data (a) and corresponding SLD profiles (b) for BCP films cast on rough substrates at T = 165°C (error bars are smaller than the data points, and have been omitted for clarity). The associated surface AFM images (c) and cartoons of the BCP orientation (d) are also provided; in all columns, the lowermost data is for a 78 nm thin film, the middle data for a 79 nm thin film, and the uppermost data for a 83 nm thin film. The SLD profiles are plotted as a function of the film normal direction, *z*, with the origin placed at the film-substrate interface. In (a), the neutron reflectivity model fits (solid line) provides excellent agreement with the experimental data (open symbols), which validates the proposed film models in (b). In particular, the Bragg peaks seen in the reflectivity profile arise due to oscillations in the SLD in the film profile, attributable to a fraction of horizontal lamellae. The intensity of the Bragg peak, and associated SLD oscillation, is noticeably larger for the 83 nm film (topmost data), indicating that at this thickness, the preferred morphology is an entirely horizontal state. In all cases, the formation of horizontal lamellae is strongly disrupted near the nanoparticle-laden substrate. (In c, the 500 nm scale bar applies to all images.)

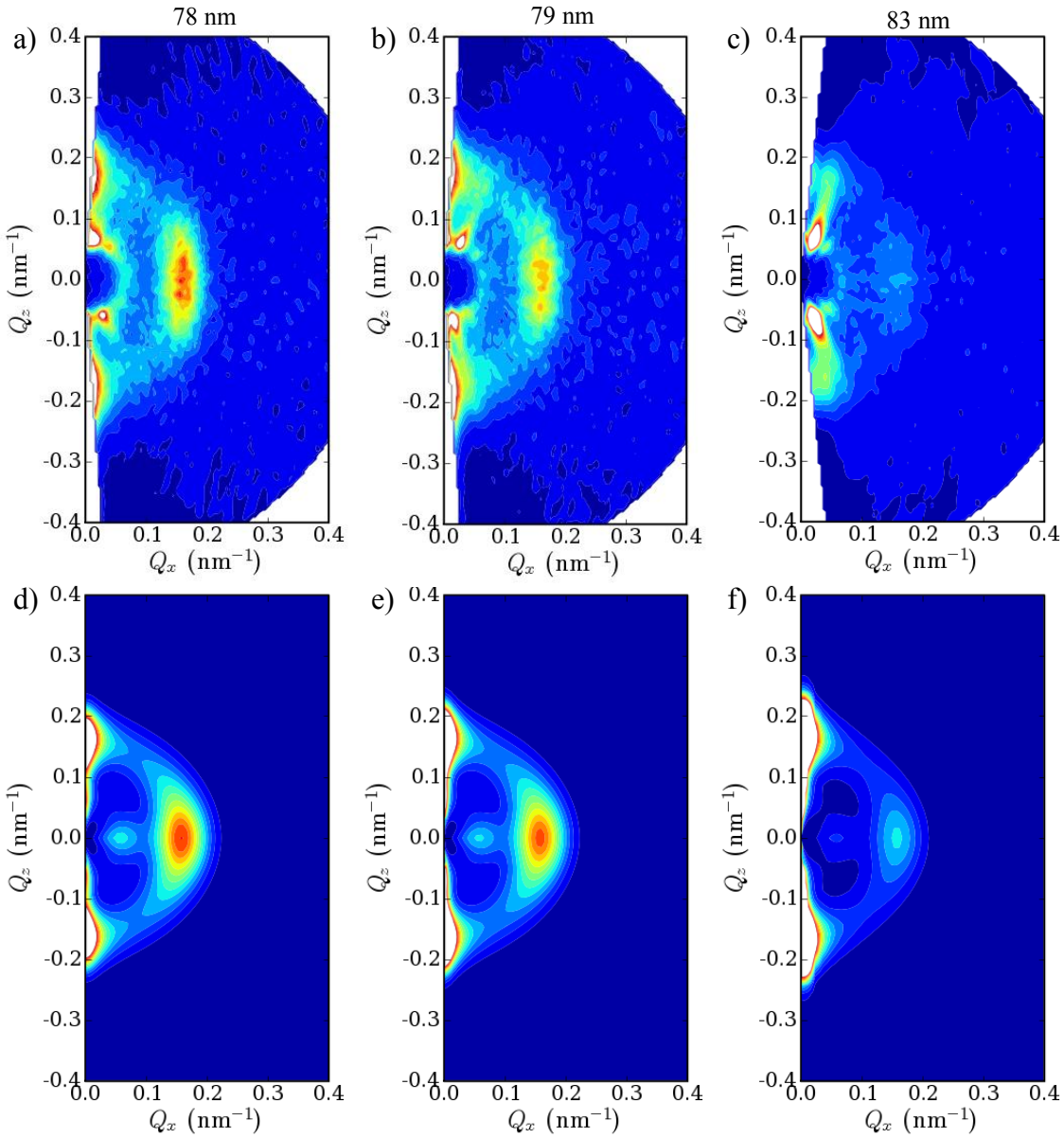


Figure 3: Reciprocal-space intensity maps generated from by accumulating SANS as a function of sample rotation angle, for annealing at 165 ºC for 18 h. All maps are plotted with the same intensity scale. The top images are experimental data, reproduced from Ref. 53 with permission from The Royal Society of Chemistry, measured on a 78 nm (a), 79 nm (b), and 83 nm (c) film. The peak at $Q_x$ = 0.16 nm$^{-1}$ is a clear signature of vertically oriented lamellae. This peak is less pronounced in (b) and nearly absent in the sample that exhibits horizontal morphology (c). The bottom images are theoretical maps based on a model including an angular distribution of lamellae, fit to 78 nm (d), 79 nm (e), and 83 nm (f). Refer to Supplementary Information for modeling procedure.

Although the neutron reflectivity data can establish a bound on the fraction of lamellae oriented horizontally, it cannot determine the orientation of the vertically oriented fraction. Similarly, the AFM measurements showing a surface fingerprint pattern cannot differentiate between strictly vertical lamellae and a cross-section through randomly oriented lamellae. In order to quantify the orientation of the self-assembled domains, we performed rotational small-angle neutron scattering (RSANS) measurements. In this technique, small-angle scattering data is accumulated as a function of sample rotation angle. By reorienting the sample, the scattering pattern becomes sensitive to order along different planes throughout the scattering volume. Figure 3 shows the scattering intensity as a function of the scattering vector, in a sample coordinate system (refer to supplementary Figure S10 for an example of the full three-dimensional reciprocal-space reconstruction). That is, the scattering along $Q_x$ corresponds to in-plane periodic structure, whereas the scattering along $Q_z$ corresponds to periodic structure in the film normal direction (similar to the neutron reflectivity experiments). Because the present samples are isotropic in-plane, $Q_x$-$Q_z$ slices of the full three-dimensional scattering, as shown in Figure 3, are sufficient.

The intense peak seen at $Q_x$ = 0.16 nm$^{-1}$ in Figure 3 (a) is a signature of in-plane order with a periodicity of 39 nm, which matches the lamellae period, $L_0$. We can further conclude that the lamellae giving rise to this peak are oriented vertically (within some angular distribution), because a completely random distribution of lamellae would instead give rise to an intense ring of uniform scattering intensity for all $Q = \sqrt{Q_x^{\ 2} + Q_z^{\ 2}} = 0.16\,\mathrm{nm}^{-1}$. The weak, diffuse scattering along that ring indicates a small portion of lamellae oriented at other angles, but the intensity of the peak clearly demonstrates a preponderance of vertically oriented lamellae. The intensity of the peak changes as a function of film thickness. In particular, the peak is nearly absent for samples that exhibit the horizontal morphology (Figure 3 c). In this regard, the SANS and neutron reflectivity data are complementary and entirely consistent: samples which exhibit a large proportion of vertical lamellae (as demonstrated by the SANS data) have a small proportion of horizontal lamellae (as demonstrated by the reflectivity data); conversely samples with a small proportion of vertical lamellae display intense oscillations in the

reflectivity data, consistent with well-defined horizontal lamellae. The intensity close to the $Q_z$ axis in the SANS maps arises from the distribution of lamellae that are oriented horizontally (within some angular distribution), and should scale inversely with the intensity of the peak from the vertical lamellae. Figure 3 d-f show fits of the experimental RSANS data (refer to supplementary material for details). This allows quantification of the relative amounts of the horizontal and vertical populations, as well as their angular spreads (Figure S9).

Representative neutron reflectivity data (and associated film profiles from best-fits) for other annealing temperatures are shown in Figure 4. Again we are able to confirm the AFM data. At high annealing temperatures (above the transition regime), the NR data has a strong Bragg peak indicative of horizontal lamellae, and the best-fit SLD profile confirms well-defined lamellae layers. At annealing temperature below the transition, there is no discernible Bragg peak. Although a one-layer model is insufficient to fully describe this data, the SLD oscillations in the best-fit are extremely weak, indicating only a very weak segregation of dPS to free surface, and PMMA to the substrate interface. Thus the surface morphology observed by AFM (Figure 1) represents the structure through the majority of the film, though not at the film-substrate interface. By adjusting thickness and annealing temperature, we can adjust lamellae orientation.

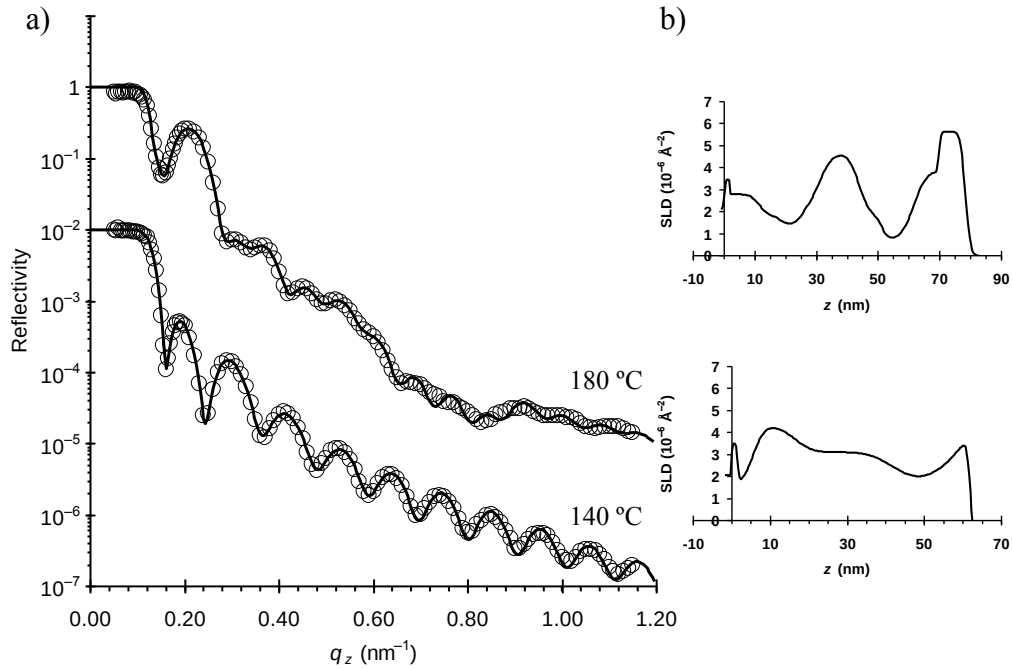


Figure 4: Neutron reflectivity data (a), including model fits (solid black lines), and corresponding SLD profiles (b) for BCP films cast on rough substrates (error bars are smaller than the data points, and have been omitted for clarity). In both (a) and (b), the lower data is for a film annealed for 4 h at 140 ºC, whereas the upper data is for a film annealed for 4 h at 180 ºC (longer time annealing data, not shown, is similar). Although the 140 ºC cannot be fit with a single-slab profile, the oscillations in the best-fit film profile are very weak; the BCP lamellae are oriented vertically, and not stratified horizontally. In comparison, the strong SLD oscillations in the 180 ºC film profile demonstrate that at this annealing temperature, the lamellae orient horizontally.

## Quantification of Surface Segregation

Although the AFM images suggest vertical states for certain film thicknesses, this technique cannot unambiguously determine whether the observed structures are truly exhibited at the surface, or are being imaged through a thin 'wetting layer.' Typically polystyrene, which has a lower surface energy, will segregate to the air surface during annealing. However this preference is weak for accessible annealing temperatures. To roughly characterize the surface interaction, we measured the surface water contact angle as a function of film thickness using a gradient thickness sample annealed in the transition region. Literature reports[60] on PS-PMMA statistical random copolymers indicate that pure PS exhibits an advancing water contact angle of about 90º, pure PMMA exhibits a contact angle of about 70º, while for a 50:50 mixture it is 82º. We observe measurable oscillations in the advancing water contact angle as a

function of thickness (refer to supplementary Figure S11), consistent with the morphology oscillation measured by AFM. Specifically, for film thickness values where the sample is horizontally-oriented, the water contact angles are consistent with a PS wetting layer; whereas for thicknesses where the vertical state is observed, the contact angles are consistent with a mixture between surface-expression of PS and PMMA. It should be noted that contact angle measurements are affected by factors besides surface chemistry; *e.g.*, roughness can alter the value appreciably. However the proposed surface expression is supported by the neutron reflectivity data, where the vertical states do not exhibit a surface SLD consistent with pure dPS, but rather have a depressed value indicating a mixture between dPS and PMMA. Combined, these measurements suggest that the preferred morphology persists to the free surface, with both chemically-distinct blocks expressed at that interface. This has implications for applications where one wants to control the average surface chemistry of a coating, where one is generating nanoscale chemical patterns, or where a component miscible in only one block needs to be available at the film surface.

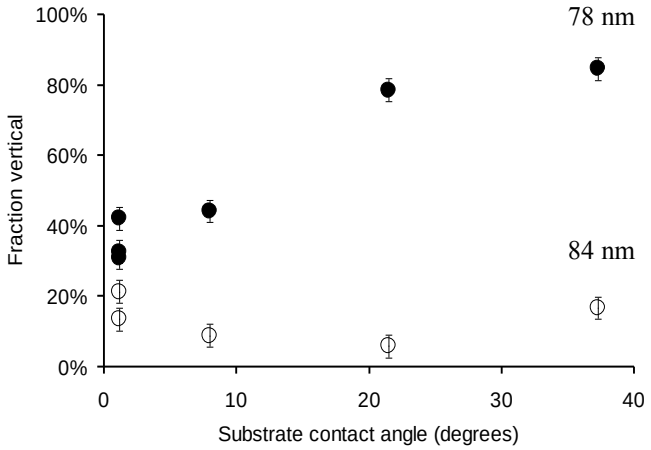


Figure 5: Effect of substrate interfacial energy on BCP orientation. Surface energy is estimated based on the average water contact angle measured on the substrate before film casting. Orientation results are for BCP thin films annealed for 4 h at 165 ºC. For a film thickness that generates predominantly vertical surface morphology (78 nm, black circles), a neutral interfacial energy generates a vertical morphology, whereas a strongly hydrophilic substrate reduces this effect and generates a conventional horizontal morphology. For a film thickness that generates predominantly horizontal morphology (84 nm, open circles), the horizontal morphology is favored regardless of interfacial energy. Error bars were estimated from the standard deviation of repeated measurements at particular film positions.

## Effective Substrate Interfacial Energy

In order to understand the nature of the temperature-dependent orientation transition described above, we altered the average surface energy of the rough substrates by changing the UV-ozone oxidation time of the nanoparticle organic coating. Samples with a gradient in surface energy were generated by exposing nanoparticle-coated substrates to a linear UV source using an acceleration stage.[61] Representative results are shown in Figure 5 for annealing in the transition regime (T = 165 $^{o}$C). For film thicknesses in which there is a horizontal orientation (open symbols), the BCP is not affected by surface energy. However in regions where the vertical morphology is possible, it is only expressed when the surface energy is closer to 'neutral', *i.e.* closer to the midpoint of pure PS and pure PMMA surface energies. This result can be easily explained: when the substrate surface energy is extremely hydrophilic, there is a strong preference for the PMMA block to segregate to that interface, generating a layer from which further horizontal lamellae will order. However if the surface energy is closer to neutral, there will be a reduced tendency for one block to segregate to that interface. For a truly neutral substrate, both blocks can wet the substrate and the BCP can adopt the vertical morphology. It is worth noting, however, that the region where vertical orientation is possible is considerably broader than would be seen on flat surfaces. In the well-studied case of random copolymer-brush treated substrates,[46, 60] the vertical orientation exists over a range of ≈ 4º in water contact angle, whereas the substrates used here yield this effectively neutral boundary condition across a ≈ 30º range of substrate water contact angle. Roughening the surface using NPs thus provides a simple and robust means of achieving a neutral boundary condition to yield vertical BCP orientations. Of course, another critical aspect is the strong segregation between the blocks, obtained by lower the processing temperature.

Figure 6 shows RSANS data for BCP lamellae assembled on rough substrates of differing surface energy. The intermediate surface energy allows for a substantial vertically-oriented lamellae population. For the samples shown in Figure 6, the annealing temperature (180 ºC) led to horizontally-oriented lamellae at the free surface. Thus the population of vertical lamellae is sub-surface. This further supports

our hypothesis that the vertically-oriented lamellae originate from the rough substrate interface, whereas the horizontal population arises from a surface-segregation layer (consistent with the NR data). For either highly hydrophilic or highly hydrophobic substrates, the vertical population is entirely suppressed from a strong preference for one of the blocks to segregate to the interface.

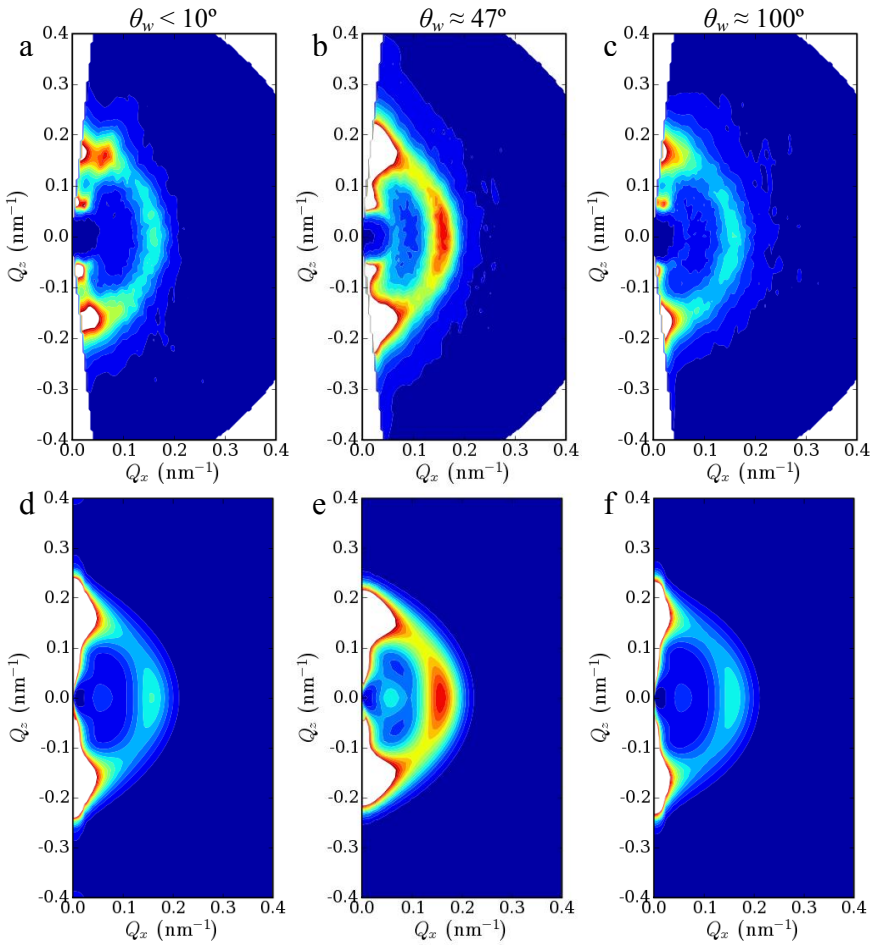


Figure 6: Reciprocal-space intensity maps from RSANS for 87 nm films annealed for 4 h at 180 ºC. All maps are plotted with the same intensity scale. The top images are experimental data, measured on BCP films cast on substrates of different average surface energy: $\theta_w < 10°$ (a), $\theta_w \approx 47°$ (b), and $\theta_w \approx 100°$ (c). At intermediate surface energy, a peak at $Q_x = 0.16$ nm$^{-1}$ appears, consistent with vertical lamellae. For extremes in surface energy the horizontal state is instead preferred. The bottom images (d–f) are corresponding fits: (d) the hydrophilic surface ($A_v = 0.30$, $s_v = 0.30$, $A_h = 0.70$, $s_h = 0.94$), (e) the intermediate surface ($A_v = 0.72$, $s_v = 0.30$, $A_h = 0.28$, $s_h = 0.75$), (f) the hydrophobic surface ($A_v = 0.40$, $s_v = 0.20$, $A_h = 0.60$, $s_h = 0.97$).

## System-specific Considerations

We now consider the origin of the orientation control seen in the surface orientation diagram. We first address aspects of the ordering peculiar to our choice of PS-*b*-PMMA material, and thereafter generalize our result using system-agnostic simulation methods. It is known that the surface energies of PS and PMMA are relatively similar and thus the segregation preference of PS to the free surface is inherently weak compared to other BCP systems (this is confirmed by the present results, where the surface PS wetting layer can be eliminated). This weaker surface-directed ordering of course makes it easier to experimentally observe the vertical orientation. The difference in surface tensions between PS and PMMA is also somewhat unusual in that it decreases with temperature[62] and the surface tensions actually become equal at sufficiently high temperature, so that a neutral boundary at the top surface can be achieved. Annealing at a temperature where there is no mismatch between the surface tensions clearly favors vertically-oriented lamellae, since there is no longer a driving force for a particular block to segregate to the free surface. For dPS-*b*-PMMA lamellae this transition is reported to occur[47] at 225 ºC (for PS-*b*-PMMA cylinders a transition at 230 ºC is reported[49]). Although this nearly-neutral boundary condition is helpful in achieving vertical orientations, this effect does not in itself explain the present observations. In particular, we still observe horizontal lamellae under many conditions; in particular when the substrate is not sufficiently 'neutral.' Thus, the substrate is playing a crucial role in directing the orientation of the BCP.

The effect of surface roughness was considered in recent work by Ranjan et al.[63] based on a simple Alexander-deGennes brush theory of the BCP layer. They concluded that the orientation of the morphology can indeed be influenced by the RMS roughness and fractal dimension of the substrate. We next consider how this might operate on a molecular level, using molecular dynamics (MD) simulations. Importantly, this simulation does not implement the special interfacial properties of PS-b-PMMA just described; thus, these MD results shed light on the generic origin of the neutral interfacial interactions arising from substrate disorder.

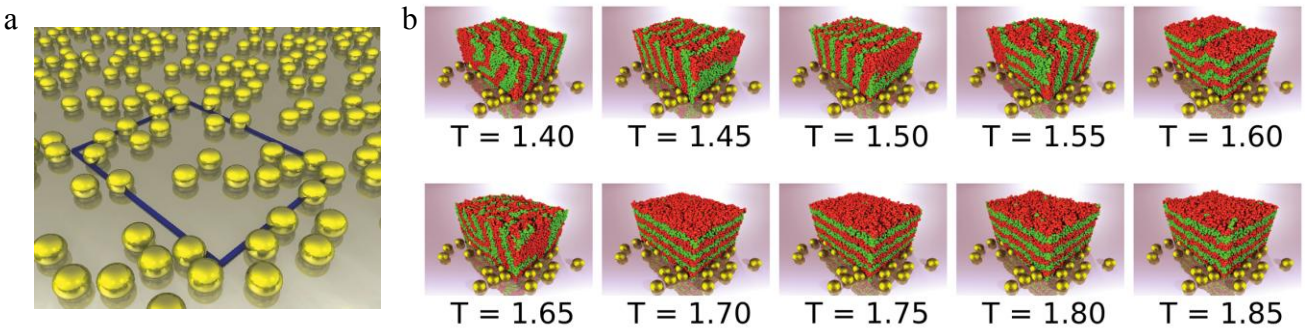


Figure 7: Results of molecular dynamics (MD) simulations. Simulations involved a substrate covered in randomly-positioned spheres (a) in order to simulate the roughness of the nanoparticle-laden substrates used experimentally. A periodic simulation box (blue rectangle) was filled with randomly oriented BCP chains and morphology allowed to evolve upon annealing. (b) Final states for a variety of annealing temperatures demonstrate a transition from vertical orientations at low temperature to horizontal at high temperature, as seen experimentally.

## *Molecular Dynamics Simulations*

We undertook molecular dynamics (MD) simulations to probe how disordered substrates influence BCP ordering. Polymer coils are simulated using a chain of beads, with two blocks of distinct chemical affinity. The chemical mismatch between two chemically distinct but covalently bound beads drives micro-phase separation. One type of bead has an energetic preference for the substrate, but we introduce randomly arranged attractive spherical nanoparticles (NP) which simulate substrate roughness (Fig. 7a). As in our previous MD work,[57] chains are initially simulated in a randomly intermixed state similar to what would be expected after spin-coating; subsequently, micro-phase separated morphologies are allowed to evolve under gradual heating and subsequent annealing (refer to Simulation Method section for details). Polymer/NP interactions were modeled using a Lennard-Jones potential. All simulation parameters are summarized in Table 1. Nanoparticle size was selected to be comparable to half the BCP

lamellar spacing ($L_0$). This is consistent with the experimental system, and indeed was found to be essential to reproduce the experimentally-observed formation of vertical lamellae.

As can be seen in Figure 7b, varying the simulated annealing temperature leads to a change in the equilibrium orientation of the BCP morphology, consistent with experiment: low temperatures lead to vertical lamellae, whereas higher temperatures lead to conventional horizontal orientation. This transition can clearly be attributed to the roughness, as simulations on flat substrates robustly gave rise to horizontal lamellae when the substrate had even a small energetic preference for one of the blocks. We evidently need to achieve two independent conditions to form a vertical orientation: a neutral boundary interaction, and sufficiently strong segregation between the BCP phases. These effects act in concert to form vertical lamellae orientations.

The fractional surface coverage of the substrate by NPs was slightly lower in the simulated system (35%), compared to the experimental system (40-50%). We found that surface coverage of ~50% in the simulation led to vertical lamellar orientations at all temperatures (supplementary Figure S12). At 35% coverage, vertical lamellae were formed at lower temperatures and there was a transition to horizontal lamellae at higher temperatures. Thus, substrate roughness drives the formation of vertical lamellae. Evidently, the NPs in the simulated system were slightly more effective in driving vertical lamellar formation than was the case for the experimental system. We note that the coarse grained simulated system was designed to capture the essential physical underpinnings of the observed physical behavior, but was not intended to reproduce quantitative features of the experimental system.

The MD simulations enable us to interrogate chain and morphology orientation in the vicinity of the substrate, so as to understand how interfacial disorder promotes a robust neutral boundary condition. We observe that the first layer of BCP chains coat the substrate and particles, consistent with their chemical affinities. The BCP layer in intimate contact with the substrate is in fact in a roughly *horizontal state*, accounting for the residual signal seen in the NR and RSANS data. However, this conformal coating does not effectively negate the disruptive effect of the NPs on the BCP orientation over lager distances; in fact, it essentially reproduces the disordered substrate topography. The defects in lamellar ordering

near the substrate then act as seeding points for vertically-oriented lamellae. Horizontal lamellae layered on these topographic defects would involve substantial distortions/bending of the lamellar morphology normal to the lamellar plane, a defective and relatively energetic state. These lamellar distortions are more strongly disfavored at lower temperatures, where the BCP segregation is stronger. This is easy to understand from the fact that the shear modulus of block-copolymer materials decreases as one approaches the order-disorder transition[64-65] (*e.g.* upon heating), at which point the block-copolymer solid becomes a liquid. At higher temperatures in a lamellar BCP, bending the morphology to conform to the nanoparticles becomes less energetically costly; thus, the lamellae orient parallel to the substrate if the temperature is raised sufficiently. Conversely, cooling the BCP increases the modulus, making the distorted horizontal states extremely disfavored. We have also recently observed an analogous transition by reducing BCP molecular mass.[66]

To illuminate this interesting disorder effect from an experimental standpoint, we measured films near the transition region (in both thickness and temperature), but with a horizontal orientation at the top surface. Using RSANS, we observe a mixed state, which includes a substantial (sometimes dominant) vertical orientation. If the substrate surface energy is shifted to be more strongly attractive to either block, then the system reverts to the usual horizontal orientation, as expected from our simulation study. Thus, we confirm that even when the free-surface drives towards horizontal lamellae, the substrate disorder can nucleate vertical orientations.

## *Discussion and Conclusion*

We have exploited interfacial roughness, engineered through adsorption of NPs, in conjunction with control of annealing temperature, to control the orientation of BCP lamellae over large areas. We observe a transition from vertical lamellae at low annealing temperature (≤ 150 ºC) to horizontal at high temperature (≥ 180 ºC), highlighting the critical role of temperature control. This transition is qualitatively similar to the surface morphology transition reported for BCP cylinders;[55] observing the effect for the lamellar phase relies on our capacity to engineer a solid substrate with nearly neutral

surface interactions over a wide range of conditions. Molecular dynamics simulations of a generic block-copolymer system illuminate the mechanism of this BCP lamellae orientational transition. Strong interfacial segregation at low temperatures makes bending around the NP surface energetically costly; the defects near the substrate interface seed the vertical orientation of the BCP lamellae. The ultimate effect of the surface disorder is to frustrate the development of orientational correlations between the lamellae and the flat silicon boundary underlying the NP layer. Thus, surface energy and temperature must be properly selected to engineer this relatively unusual BCP orientation.

By combining AFM, NR, and rotational SANS, we have addressed the difficult problem of quantifying both the surface morphology and the three-dimensional orientational distribution of lamellae within these films. This is a general measurement strategy that can be applied to any nanostructured films that give rise to scattering peaks, and the tools we describe are transferable to many other systems and problems. Our analysis demonstrates that the vertical state has a relatively small angular spread (it is not isotropic), though it is not as well-aligned as a horizontal state (which must necessarily align with the substrate). Furthermore the vertical orientation does not have a surface-wetting layer; both chemically-distinct blocks are expressed at the free surface. This has implications for applications in which one wants to control the average surface chemistry of a coating, or where one wants to create nano-scale chemical patterns.

In previous work, we explored the effect of varying both temperature and molecular mass on the formation of in-plane interfacial patterns in horizontal lamellae systems.[67-69] In these experiments, it was found that increasing BCP segregation strength, either by lowering the temperature or by increasing the molecular mass, reduced the size of surface patterns (holes, islands and 'spinodal' patterns depending on block copolymer film thickness), due to the increased elastic energetics of deforming the lamellae under stronger segregation conditions. In this work, we again find evidence of this coupling between segregation strength and BCP ordering.

Finally, we note that there is another strategy for increasing the thermodynamic driving force $\chi N$ to enhance BCP ordering in thin films: the introduction of additives having a selective affinity for one of

the block components.[70-72] This approach to increasing segregation strength and the 'quality' of block-copolymer ordering has been demonstrated in a number of bock-copolymer materials.[72-76] Increasing $\chi N$ by using larger molecular mass materials has the disadvantage of also increasing the BCP repeat-spacing, while decreasing temperature reduces ordering rates, and may affect the quality of ordering due to dynamic heterogeneity.[77] Thus, using additives to increase segregation, in combination with the tuning of substrate interactions described herein, may be a valuable future strategy for engineering block-copolymer morphology orientation. Overall, our results point towards a general motif for controlling the order in self-assembling polymer films: to tune the material segregation, and thus mechanical properties, in order that the coupling to substrate topography drives towards desired ordering.

## *Experimental*

### Nanoparticle Preparation

Silica nanoparticles (diameter = 20 nm) in a colloidal dispersion (mass fraction 30 %, suspension in methyl isobutyl ketone (MIBK)) were obtained from Nissan Chemical Industries, Ltd.[78] and dried over anhydrous $MgSO_4$. The nanoparticle surface modification was carried out according to a modified procedure reported in the literature.[79] Magnesium sulfate, hexane, methanol, and 1,1,1,3,3,3 hexamethyldisilazane (HMDS) were obtained from Aldrich and used without further purification. The n-propyldimethylchlorosilane was obtained from Gelest. The MIBK/nanoparticle dispersion (10 g) was filtered and transferred to a 250 mL round bottom flask under argon. The n-propyldimethylchlorosilane (3 mL) was added dropwise *via* syringe. The reaction mixture was stirred overnight at 50 ºC and allowed to cool to room temperature before adding 6 mL of the HMDS. The reaction was then stirred at room temperature for 3 h, and heated to 50 ºC for 8 h. The white precipitate which formed upon the addition of HMDZ was removed *via* centrifugation. The orange dispersion was precipitated *via* dropwise addition into a methanol:water mixture (4:1 by volume). The particles were centrifuged and the supernatant decanted. The recovered particles were then dissolved in THF and precipitated in a

methonal:water mixture (repeated 3 times). The particles were then dried at 70 ºC overnight under vacuum to yield a yellowish powder. The hydrophobic nanoparticles are soluble in organic solvents (THF, chloroform, etc.), with mild sonication (300 s) achieving full dispersion.

## Sample Preparation

Substrates were polished Si wafers cleaned using warm piranha solution (mixture of 30 % volume fraction $H_2O_2$ and concentrated $H_2SO_4$ in a 1:3 ratio) for 20 minutes. The silica nanoparticles were cast onto the Si substrates by spin-coating from chloroform solutions. The particle coverage depends strongly on solution concentration and more weakly on spin-coating velocity. To achieve partial substrate coverage, a solution of nanoparticles in chloroform (mass fraction 0.04 %) was cast at 126 rad/s for 30 s. These surfaces have root-mean-square (rms) roughness 10 nm (as measured by AFM). The estimated 2D areal coverage of the fractal-like aggregates depends somewhat on definition (e.g. thresholding). An upper bound for the coverage of 51% can be estimated based on a >1 nm extension of the AFM topography above the lowest-lying flat regions, whereas we estimate ≈ 40% coverage using a height cutoff of 10 nm. Samples were oxidized by placing in an ultraviolet (UV) ozone chamber, with exposure time (0 s to 600 s) controlling final surface energy. The UV light generates ozone and atomic oxygen in the vicinity of the substrate, which oxidize the sample, converting organic $CH_2$ and $CH_3$ groups progressively into more hydrophilic groups (*e.g.*, $CH_2OH$ and COOH), as confirmed by x-ray photoelectron spectroscopy (XPS), and consistent with literature.[80] Samples with gradients in the nanoparticle surface energy were generated by accelerating the sample beneath a linear UV light-source.[61] The UV radiation emitted from the light-source slit generates ozone and atomic oxygen in the vicinity, which oxidize the sample. The total oxidation being dependent on UV exposure time, sample acceleration generates a corresponding gradient in total oxidation time, hence surface energy.

The diblock-copolymer was symmetric poly(deuterated styrene-*block*-methyl methacrylate) (dPS-*b*-PMMA), with a molar mass of 62.6 kg/mol (29.5 kg/mol styrene and 33.1 kg/mol methyl methacrylate), and polydispersity of ≈ 1.14 (Polymer Source, Inc.). This BCP forms lamellae with a bulk period $L_0$ = 39 nm (as measured by SANS, and consistent with AFM data). Thin films were prepared by casting from

toluene, using either spin-coating (solution mass fraction 1.5 %, 100 rad/s to 210 rad/s, depending on desired thickness, for 45 s) or flow-coating (solution mass fraction 3 %, 8 mm/s to 40 mm/s sweep speed, depending on desired thickness). Combinatorial samples with a gradient in thickness were prepared using the flow-coating acceleration technique previously reported,[81] with a blade height of 200 $\mu$m, an acceleration of 1 mm/s$^2$ to 10 mm/s$^2$ (depending on desired thickness range). The BCP films, coated onto silica nanoparticle substrates, were then annealed in a vacuum oven.

One of the advantages of combinatorial techniques is that all other aspects of sample history (preparation conditions, thermal history, etc.) are constant for the entire sample. Nevertheless, in some cases it is possible that the observed effects arise from the combinatorial sample preparation itself (*e.g.* the particular shear-flow pattern of flow-coating). However it was observed that the film morphologies were not dependant on the preparation method. Thickness gradients obtained with different accelerations exhibited morphology oscillations at the same thickness values. Moreover, samples with uniform thickness, prepared either *via* flow-coating at constant velocity, or spin-casting, exhibited the same morphology orientation for particular thickness values

## Atomic Force Microscopy

Sample surfaces were imaged using atomic force microscopy (AFM) in the intermittent contact ('tapping') mode using an Asylum MFP3D instrument. The images were then segmented by software methods[53] into regions of parallel and perpendicular lamellae (supplementary Figure S6). Segmentation analysis was performed using the IGOR Pro (Wavemetrics) programming environment. Both phase and amplitude AFM images were analyzed, giving comparable results. The images (512 pixels by 512 pixels) were flattened (1$^{st}$-order polynomial) and segmented by calculating local absolute gradients, and using a threshold to differentiate between regions with large absolute gradients (indicative of small-scale patterns arising from perpendicular lamellae) and regions with shallow gradients (indicative of flat parallel lamellae). Similar procedures have been previously used to generate maps of BCP cylinder orientations.[33, 82] A fraction of vertical lamellae (versus horizontal lamellae), $f_v$, was calculated based on

the relative segmented areas in the images. This segmentation produces an error of ± 3 %, based on the standard deviation of repeated measurements conducted at the same film location.[83]

Film thickness was measured by taking AFM images across a scratch in the film created with a razor blade. For thickness gradient samples, multiple measurements along the gradient were used to generate a calibration between position and thickness. The high-resolution images were then acquired near this calibration line. For films with an underlying nanoparticle layer, reported value is the total film thickness, which includes the BCP film and the underlying nanoparticle layer. Since this nanoparticle layer is inherently rough, it is difficult to define its thickness. However, comparison of samples cast on bare Si versus those cast on nanoparticle-coated substrates indicates that the nanoparticle layer contributes, statistically, ≈ 12 nm to the overall thickness. This thickness offset was also confirmed by comparing the location of the 'islands and holes' regions on samples cast on bare wafers to the equivalent nanoparticle-coated samples.

## Neutron Reflectometry

Neutron reflectivity experiments were performed using the NG7 instrument at the National Institute of Standards and Technology Center for Neutron Research. Specular-mode measurements were performed using neutrons of wavelength $\lambda$ = 0.476 nm. The momentum transfer, $q_z = (4\pi/\lambda)\sin\theta$, was varied between 0.05 $nm^{-1}$ and 1.5 $nm^{-1}$ by varying the specular reflection angle, $\theta$. The instrument resolution was $\Delta q_z / q_z = 0.04$. Background was eliminated by performing scans with the sample angle offset from the specular condition, and subtracting the average of these scans from the data. The detector count time was varied as a function of angle to maintain uniform and reasonable statistic over the entire scan region. The data were normalized to the measured intensity of the incident beam. The normalized reflectivity curves were fit to scattering length density (SLD) profiles using the NRSA software,[84] where a free-form film profile is approximated as a sum of Chebyshev polynomials, and a modified simulated annealing algorithm minimizes the error. Fits were also performed using the Yanera software,[85] which implements Parratt's dynamic approach,[86] using a multi-slab model for the film profile, and a variety of minimization algorithms. Both fitting procedures produced similar results.

## Small-Angle Neutron Scattering

Small-angle neutron scattering (SANS) experiments were performed using the NG7-SANS instrument at the NIST center for Neutron Research, using an incident neutron beam of wavelength $\lambda$ = 0.8 nm ($\Delta\lambda/\lambda = 0.11$). Scans were performed as a function of sample rotation angle, $\omega$, in the range –86º to +86º. The SANS intensity maps were separated into $q_x$ and $q_y$ components, which are the scattering vectors in the coordinate system of the incident beam, where the $z$-axis points towards the source, and the $y$-axis points along the sample rotation vector. The $q_y$ intensities do not vary with sample rotation, and were used to normalize the intensity of the data. The normalized data was rotated into a coordinate system aligned with the sample, which is denoted by ($Q_x$, $Q_z$). In this coordinate system, the $z$-axis points along the normal of the thin film, and the sample lies in the $x$-$y$ plane.

## Molecular Dynamics Simulations

Our molecular dynamics simulation model builds upon our previously-reported[57] model of a thin block copolymer film in contact with an attractive substrate. Polymers are modeled as linear chains of coarse-grained beads of two distinct types, which are segregated lengthwise along the chain into two equal blocks in order to select the lamellar region of the BCP phase diagram. Because each bead type is parameterized with a unique self-cohesive interaction strength, the simulated chains spontaneously microphase separate given sufficient simulation time. Due to cohesive interactions between polymer beads and underfilling of the simulation box, the model film spontaneously forms a free surface with an overlying vacuum phase. Our present simulations use the same bead-bead interaction parameters as in our previous work. However, here we add an additional bead type to simulate the nanoparticles coating the substrate. The NP/polymer interaction was modeled using a Lennard-Jones potential. Simulation interaction parameters are provided in Table 1, in reduced units based on the characteristic length, $l^*$ = 1 nm, and the characteristic energy, $\varepsilon^*$ = 4.1 pN•nm (the thermal energy available at room temperature).

Our model system comprises 5,280 identically parameterized chains, each with a total of 10 beads. A total of 17 nanoparticles were randomly placed along the substrate in non-overlapping fashion as shown in Fig 11, yielding a fractional coverage of ~35%. Nanoparticles were held fixed during simulations. For

each simulation run, an initial disordered film structure was formed by a pre-production simulation run of 100,000 molecular dynamics steps in which bead-bead interaction energies were ramped from zero to the final values listed in Table I. A spring force was applied during this stage to prevent the film from losing cohesion and detaching from the substrate in the absence of cohesive interactions. Subsequently, films were heated for 2,000,000 MD steps, with the temperature linearly ramped from the initial temperature (1.2 reduced temperature units) to a unique annealing temperature. Ten annealing temperatures in reduced units were considered: 1.40, 1.45, 1.50, 1.55, 1.60, 1.65, 1.70, 1.75, and 1.80. All of these annealing temperatures are well above the glass-transition temperatures of either of the polymer blocks (supplementary Figure S13). Each system was held at its unique annealing temperature for 8,000,000 MD steps. Coordinates were saved every 50,000 MD steps.

Simulations were performed using the LAMMPS package[87] made available by Sandia National Laboratories using the canonical (NVT) ensemble and a reduced time step of 0.005. The x,y, (in plane) and z (out of plane) dimensions of the simulation cell in reduced length units were 45.7, 35, and 49.5, respectively. Periodic boundary conditions were applied in the film (x-y) plane. Care was taken to insure that the simulation volume was large enough to avoid artifacts arising from commensurability between the BCP repeat spacing and the box dimensions. This can be confirmed both by the smooth variation of system properties as a function of temperature (since $L_0$ depends on temperature, varying temperature inherently varies any $L_0$/boxsize commensurability condition), and by the insensitivity of morphology to boxsize. Horizontal lamellae are effectively unconstrained in the simulation (free surface), while vertical lamellae are able to rotate in the x,y plane in order to accommodate any $L_0$/boxsize ratio. The substrate was set to have an energetic preference for one of the two blocks. The nanoparticles were also parameterized to have an energetic preference for the same block as the substrate, consistent with the experimental system. Nanoparticles diameter was selected to be comparable to half the lamellar repeat length, $L_0$, consistent with the experimental system. As discussed in the Results section, this is essential for the formation of vertical lamellae.

**TABLE 1. Simulation Interaction Parameters**

**Polymer Bead / Polymer Bead Interactions**

| type | parameter | value |
|---|---|---|
| bond stretching | $l_o$ | 1 |
| | $k_{stretch}$ | 500 |
| Lennard-Jones | | |
| | $\varepsilon_{AA}$ | 1.9 |
| | $\sigma_{AB}$ | 0.8 |
| | $\varepsilon_{BB}$ | 1.6 |
| | $\sigma_{polymer/polymer}$ | 0.84 |

**Polymer Bead / Nanoparticle Interactions**

| type | parameter | value |
|---|---|---|
| Lennard-Jones | | |
| | $\varepsilon_{A/NP}$ | 3.5 |
| | $\varepsilon_{B/NP}$ | 2.5 |
| | $\sigma_{polymer/NP}$ | 3.39 |

**Polymer Bead / Substrate Interactions**

| type | parameter | value |
|---|---|---|
| Lennard-Jones | | |
| | $\varepsilon_{A/Substrate}$ | 4.5 |
| | $\varepsilon_{B/Substrate}$ | 0.75 |

## *Acknowledgments*

Work carried out in part in the Center for Functional Nanomaterials, Brookhaven National Laboratory, which is supported by the U.S. Department of Energy, Office of Basic Energy Sciences, under Contract No. DE-AC02-98CH10886. We thank the Division of Electrical and Software Engineering (FDA) for use of the high performance computing facilities and the Division of Imaging and Applied Mathematics (FDA) for additional computational time.

REFERENCES

1. Fasolka, M. J.; Mayes, A. M., Block Copolymer Thin Films: Physics and Applications. *Annu. Rev. Mater. Res.* **2001,** *31*, 323-355.
2. Hawker, C. J.; Russell, T. P., Block Copolymer Lithography: Merging "Bottom-up" with "Top-Down" Processes. *Mrs Bull* **2005,** *30*, 952-966.
3. Stoykovich, M. P.; Nealey, P. F., Block Copolymers and Conventional Lithography. *Mater. today* **2006,** *9*, 20.
4. Li, M.; Ober, C. K., Block Copolymer Patterns and Templates. *Mater. today* **2006,** *9*, 30.

5. Christopher, H.; Miri, P.; Paul, M. C.; Richard, A. R.; Douglas, H. A., Lithography with a Mask of Block Copolymer Microstructures. *Journal of Vacuum Science & Technology B: Microelectronics and Nanometer Structures* **1998,** *16*, 544-552.
6. Segalman, R. A., Patterning with Block Copolymer Thin Films. *Materials Science and Engineering: R: Reports* **2005,** *48*, 191-226.
7. Kim, H.-C.; Park, S.-M.; Hinsberg, W. D., Block Copolymer Based Nanostructures: Materials, Processes, and Applications to Electronics. *Chem. Rev.* **2009,** *110*, 146-177.
8. Cheng, J. Y.; Mayes, A. M.; Ross, C. A., Nanostructure Engineering by Templated Self-Assembly of Block Copolymers. *Nat Mater* **2004,** *3*, 823-828.
9. Marencic, A. P.; Register, R. A., Controlling Order in Block Copolymer Thin Films for Nanopatterning Applications. *Annual Review of Chemical and Biomolecular Engineering* **2010,** *1*, 277-297.
10. Hamley, I. W., Ordering in Thin Films of Block Copolymers: Fundamentals to Potential Applications. *Prog. Polym. Sci.* **2009,** *34*, 1161-1210.
11. Darling, S. B., Directing the Self-Assembly of Block Copolymers. *Prog. Polym. Sci.* **2007,** *32*, 1152-1204.
12. Riise, B. L.; Fredrickson, G. H.; Larson, R. G.; Pearson, D. S., Rheology and Shear-Induced Alignment of Lamellar Diblock and Triblock Copolymers. *Macromol.* **1995,** *28*, 7653-7659.
13. Koppi, K. A.; Tirrell, M.; Bates, F. S., Shear-Induced Isotropic-to-Lamellar Transition. *Phys. Rev. Lett.* **1993,** *70*, 1449.
14. Ashok, B.; Muthukumar, M.; Russell, T. P., Confined Thin Film Diblock Copolymer in the Presence of an Electric Field. *J. Chem. Phys.* **2001,** *115*, 1559-1564.
15. Pereira, G. G.; Williams, D. R. M., Diblock Copolymer Melts in Electric Fields: The Transition from Parallel to Perpendicular Alignment Using a Capacitor Analogy. *Macromol.* **1999,** *32*, 8115-8120.
16. Tsori, Y.; Andelman, D., Thin Film Diblock Copolymers in Electric Field: Transition from Perpendicular to Parallel Lamellae. *Macromol.* **2002,** *35*, 5161-5170.
17. Kim, S. H.; Misner, M. J.; Russell, T. P., Solvent-Induced Ordering in Thin Film Diblock Copolymer/Homopolymer Mixtures. *Adv. Mater.* **2004,** *16*, 2119-2123.
18. Kimura, M.; Misner, M. J.; Xu, T.; Kim, S. H.; Russell, T. P., Long-Range Ordering of Diblock Copolymers Induced by Droplet Pinning. *Langmuir* **2003,** *19*, 9910-9913.
19. Hashimoto, T.; Koizumi, S.; Hasegawa, H., Ordered Structure in Blends of Block Copolymers.2.Self-Assembly for Immiscible Lamella-Forming Copolymers. *Macromol.* **1994,** *27*, 1562-1570.
20. Abetz, V.; Goldacker, T., Formation of Superlattices Via Blending of Block Copolymers. *Macromol. Rapid Commun.* **2000,** *21*, 16-34.
21. Spontak, R. J.; Fung, J. C.; Braunfeld, M. B.; Sedat, J. W.; Agard, D. A.; Kane, L.; Smith, S. D.; Satkowski, M. M.; Ashraf, A.; Hajduk, D. A.; Gruner, S. M., Phase Behavior of Ordered Diblock Copolymer Blends: Effect of Compositional Heterogeneity. *Macromol.* **1996,** *29*, 4494-4507.
22. Yager, K. G.; Lai, E.; Black, C. T., Self-Assembled Phases of Block Copolymer Blend Thin Films. *ACS Nano* **2014,** *8*, 10582-10588.
23. Bodycomb, J.; Funaki, Y.; Kimishima, K.; Hashimoto, T., Single-Grain Lamellar Microdomain from a Diblock Copolymer. *Macromol.* **1999,** *32*, 2075-2077.
24. De Rosa, C.; Park, C.; Thomas, E. L.; Lotz, B., Microdomain Patterns from Directional Eutectic Solidification and Epitaxy. *Nature* **2000,** *405*, 433.
25. Cheolmin, P.; Joy, Y. C.; Michael, J. F.; Anne, M. M.; Ross, C. A.; Edwin, L. T.; Claudio De, R., Double Textured Cylindrical Block Copolymer Domains Via Directional Solidification on a Topographically Patterned Substrate. *Appl. Phys. Lett.* **2001,** *79*, 848-850.
26. Hashimoto, T.; Bodycomb, J.; Funaki, Y.; Kimishima, K., The Effect of Temperature Gradient on the Microdomain Orientation of Diblock Copolymers Undergoing an Order-Disorder Transition. *Macromol.* **1999,** *32*, 952-954.

27. Mita, K.; Tanaka, H.; Saijo, K.; Takenaka, M.; Hashimoto, T., Cylindrical Domains of Block Copolymers Developed Via Ordering under Moving Temperature Gradient. *Macromol.* **2007,** *40*, 5923-5933.
28. Mita, K.; Tanaka, H.; Saijo, K.; Takenaka, M.; Hashimoto, T., Ordering of Cylindrical Domain of Block Copolymers under Moving Temperature Gradient: Effects of Moving Rate. *Macromol.* **2008,** *41*, 6780-6786.
29. Mita, K.; Tanaka, H.; Saijo, K.; Takenaka, M.; Hashimoto, T., Ordering of Cylindrical Domains of Block Copolymers under Moving Temperature Gradient: Separation of T-Induced Ordering from Surface-Induced Ordering. *Macromol.* **2008,** *41*, 6787-6792.
30. Mita, K.; Takenaka, M.; Hasegawa, H.; Hashimoto, T., Cylindrical Domains of Block Copolymers Developed Via Ordering under Moving Temperature Gradient: Real-Space Analysis. *Macromol.* **2008,** *41*, 8789-8799.
31. Mita, K.; Tanaka, H.; Saijo, K.; Takenaka, M.; Hashimoto, T., Macroscopically Oriented Lamellar Microdomains Created by "Cold Zone-Heating" Method Involving Oot. *Polymer* **2008,** *49*, 5146-5157.
32. Angelescu, D. E.; Waller, J. H.; Adamson, D. H.; Register, R. A.; Chaikin, P. M., Enhanced Order of Block Copolymer Cylinders in Single-Layer Films Using a Sweeping Solidification Front. *Adv. Mater.* **2007,** *19*, 2687-2690.
33. Berry, B. C.; Bosse, A. W.; Douglas, J. F.; Jones, R. L.; Karim, A., Orientational Order in Block Copolymer Films Zone Annealed Below the Order-Disorder Transition Temperature. *Nano Lett.* **2007,** *7*, 2789-2794.
34. Yager, K. G.; Fredin, N. J.; Zhang, X.; Berry, B. C.; Karim, A.; Jones, R. L., Evolution of Block-Copolymer Order through a Moving Thermal Zone. *Soft Matter* **2010,** *6*, 92-99.
35. Singh, G.; Yager, K. G.; Berry, B.; Kim, H.-C.; Karim, A., Dynamic Thermal Field-Induced Gradient Soft-Shear for Highly Oriented Block Copolymer Thin Films. *ACS Nano* **2012,** *6*, 10335-10342.
36. Singh, G.; Yager, K. G.; Smilgies, D.-M.; Kulkarni, M. M.; Bucknall, D. G.; Karim, A., Tuning Molecular Relaxation for Vertical Orientation in Cylindrical Block Copolymer Films Via Sharp Dynamic Zone Annealing. *Macromol.* **2012,** *45*, 7107-7117.
37. Majewski, P. W.; Yager, K. G., Millisecond Ordering of Block Copolymer Films Via Photothermal Gradients. *ACS Nano* **2015,** *accepted*, doi: 10.1021/nn5071827.
38. Segalman, R. A.; Hexemer, A.; Kramer, E. J., Effects of Lateral Confinement on Order in Spherical Domain Block Copolymer Thin Films. *Macromol.* **2003,** *36*, 6831-6839.
39. Sundrani, D.; Darling, S. B.; Sibener, S. J., Guiding Polymers to Perfection: Macroscopic Alignment of Nanoscale Domains. *Nano Lett.* **2003,** *4*, 273-276.
40. Sundrani, D.; Darling, S. B.; Sibener, S. J., Hierarchical Assembly and Compliance of Aligned Nanoscale Polymer Cylinders in Confinement. *Langmuir* **2004,** *20*, 5091-5099.
41. Hammond, M. R.; Cochran, E.; Fredrickson, G. H.; Kramer, E. J., Temperature Dependence of Order, Disorder, and Defects in Laterally Confined Diblock Copolymer Cylinder Monolayers. *Macromol.* **2005,** *38*, 6575-6585.
42. Ruiz, R.; Ruiz, N.; Zhang, Y.; Sandstrom, R. L.; Black, C. T., Local Defectivity Control of 2d Self-Assembled Block Copolymer Patterns. *Adv. Mater.* **2007,** *19*, 2157-2162.
43. Zhang, X.; De Paoli Lacerda, S. H.; Yager, K. G.; Berry, B. C.; Douglas, J. F.; Jones, R. L.; Karim, A., Target Patterns Induced by Fixed Nanoparticles in Block Copolymer Films. *ACS Nano* **2009,** *3*, 2115-2120.
44. Yang, X. M.; Peters, R. D.; Nealey, P. F.; Solak, H. H.; Cerrina, F., Guided Self-Assembly of Symmetric Diblock Copolymer Films on Chemically Nanopatterned Substrates. *Macromol.* **2000,** *33*, 9575-9582.
45. Ouk Kim, S.; Solak, H. H.; Stoykovich, M. P.; Ferrier, N. J.; de Pablo, J. J.; Nealey, P. F., Epitaxial Self-Assembly of Block Copolymers on Lithographically Defined Nanopatterned Substrates. *Nature* **2003,** *424*, 411.

46. Mansky, P.; Russell, T. P.; Hawker, C. J.; Pitsikalis, M.; Mays, J., Ordered Diblock Copolymer Films on Random Copolymer Brushes. *Macromolecules* **1997,** *30*, 6810-6813.
47. Mansky, P.; Russell, T. P.; Hawker, C. J.; Mays, J.; Cook, D. C.; Satija, S. K., Interfacial Segregation in Disordered Block Copolymers: Effect of Tunable Surface Potentials. *Phys. Rev. Lett.* **1997,** *79*, 237.
48. Huang, E.; Rockford, L.; Russell, T. P.; Hawker, C. J., Nanodomain Control in Copolymer Thin Films. *Nature* **1998,** *395*, 757.
49. Han, E.; Stuen, K. O.; Leolukman, M.; Liu, C.-C.; Nealey, P. F.; Gopalan, P., Perpendicular Orientation of Domains in Cylinder-Forming Block Copolymer Thick Films by Controlled Interfacial Interactions. *Macromol.* **2009,** *42*, 4896-4901.
50. Sivaniah, E.; Hayashi, Y.; Matsubara, S.; Kiyono, S.; Hashimoto, T.; Kukunaga, K.; Kramer, E. J.; Mates, T., Symmetric Diblock Copolymer Thin Films on Rough Substrates. Kinetics and Structure Formation in Pure Block Copolymer Thin Films. *Macromol.* **2005,** *38*, 1837-1849.
51. Tsori, Y.; Sivaniah, E.; Andelman, D.; Hashimoto, T., Orientational Transitions in Symmetric Diblock Copolymers on Rough Surfaces. *Macromol.* **2005,** *38*, 7193-7196.
52. Sivaniah, E.; Hayashi, Y.; Iino, M.; Hashimoto, T.; Fukunaga, K., Observation of Perpendicular Orientation in Symmetric Diblock Copolymer Thin Films on Rough Substrates. *Macromol.* **2003,** *36*, 5894-5896.
53. Yager, K. G.; Berry, B. C.; Page, K.; Patton, D.; Karim, A.; Amis, E. J., Disordered Nanoparticle Interfaces for Directed Self-Assembly. *Soft Matter* **2009,** *5*, 622-628.
54. Kulkarni, M. M.; Yager, K. G.; Sharma, A.; Karim, A., Combinatorial Block Copolymer Ordering on Tunable Rough Substrates. *Macromol.* **2012,** *45*, 4303-4314.
55. Zhang, X.; Berry, B. C.; Yager, K. G.; Kim, S.; Jones, R. L.; Satija, S.; Pickel, D. L.; Douglas, J. F.; Karim, A., Surface Morphology Diagram for Cylinder-Forming Block Copolymer Thin Films. *ACS Nano* **2008,** *2*, 2331-2341.
56. Ji, S.; Liu, C.-C.; Son, J. G.; Gotrik, K.; Craig, G. S. W.; Gopalan, P.; Himpsel, F. J.; Char, K.; Nealey, P. F., Generalization of the Use of Random Copolymers to Control the Wetting Behavior of Block Copolymer Films. *Macromolecules* **2008,** *41*, 9098-9103.
57. Forrey, C.; Yager, K. G.; Broadaway, S. P., Molecular Dynamics Study of the Role of the Free Surface on Block Copolymer Thin Film Morphology and Alignment. *ACS Nano* **2011,** *5*, 2895-2907.
58. Kim, S.; Nealey, P. F.; Bates, F. S., Decoupling Bulk Thermodynamics and Wetting Characteristics of Block Copolymer Thin Films. *ACS Macro Letters* **2011,** *1*, 11-14.
59. Huang, E.; Mansky, P.; Russell, T. P.; Harrison, C.; Chaikin, P. M.; Register, R. A.; Hawker, C. J.; Mays, J., Mixed Lamellar Films: Evolution, Commensurability Effects, and Preferential Defect Formation. *Macromol.* **1999,** *33*, 80-88.
60. Mansky, P.; Liu, Y.; Huang, E.; Russell, T. P.; Hawker, C., Controlling Polymer-Surface Interactions with Random Copolymer Brushes. *Science* **1997,** *275*, 1458-1460.
61. Berry, B. C.; Stafford, C. M.; Pandya, M.; Lucas, L. A.; Karim, A.; Fasolka, M. J., Versatile Platform for Creating Gradient Combinatorial Libraries Via Modulated Light Exposure. *Rev Sci Instrum* **2007,** *78*, 072202.
62. Brandrup, J.; Immergut, E. H.; Grulke, E. A., *Polymer Handbook, 4th Ed*. John Wiley and Sons: New York, 1999.
63. Ranjan, A.; Kulkarni, M.; Karim, A.; Sharma, A., Diblock Copolymer Lamellae on Sinusoidal and Fractal Surfaces. *The Journal of Chemical Physics* **2012,** *136*, 094903-9.
64. Han, C. D.; Baek, D. M.; Kim, J. K.; Ogawa, T.; Sakamoto, N.; Hashimoto, T., Effect of Volume Fraction on the Order-Disorder Transition in Low Molecular Weight Polystyrene-Block-Polyisoprene Copolymers. 1. Order-Disorder Transition Temperature Determined by Rheological Measurements. *Macromol.* **1995,** *28*, 5043-5062.
65. Bates, F. S.; Rosedale, J. H.; Fredrickson, G. H., Fluctuation Effects in a Symmetric Diblock Copolymer near the Order–Disorder Transition. *The Journal of Chemical Physics* **1990,** *92*, 6255-6270.

66. Zhang, X.; Douglas, J. F.; Satija, S.; Karim, A., Enhanced Vertical Ordering of Block Copolymer Films by Tuning Molecular Mass. *RSC Advances* **2015,** *5*, 32307-32318.
67. Smith, A. P.; Douglas, J. F.; Meredith, J. C.; Amis, E. J.; Karim, A., Combinatorial Study of Surface Pattern Formation in Thin Block Copolymer Films. *Phys. Rev. Lett.* **2001,** *87*, 015503.
68. Smith, A. P.; Douglas, J. F.; Meredith, J. C.; Amis, E. J.; Karim, A., High-Throughput Characterization of Pattern Formation in Symmetric Diblock Copolymer Films. *Journal of Polymer Science Part B: Polymer Physics* **2001,** *39*, 2141-2158.
69. Smith, A. P.; Douglas, J. F.; Amis, E. J.; Karim, A., Effect of Temperature on the Morphology and Kinetics of Surface Pattern Formation in Thin Block Copolymer Films. *Langmuir* **2007,** *23*, 12380-12387.
70. Dudowicz, J.; Freed, K. F.; Douglas, J. F., Modification of the Phase Stability of Polymer Blends by Diblock Copolymer Additives. *Macromol.* **1995,** *28*, 2276-2287.
71. Huang, C.-I.; Lodge, T. P., Self-Consistent Calculations of Block Copolymer Solution Phase Behavior. *Macromol.* **1998,** *31*, 3556-3565.
72. Bosse, A. W.; Tirumala, V. R.; Lin, E. K., Tuning Block Copolymer Phase Behavior with a Selectively Associating Homopolymer Additive. *Journal of Polymer Science Part B: Polymer Physics* **2009,** *47*, 2083-2090.
73. Wang, J.-Y.; Chen, W.; Roy, C.; Sievert, J. D.; Russell, T. P., Influence of Ionic Complexes on Phase Behavior of Polystyrene-B-Poly(Methyl Methacrylate) Copolymers. *Macromol.* **2008,** *41*, 963-969.
74. Wang, J.-Y.; Chen, W.; Russell, T. P., Ion-Complexation-Induced Changes in the Interaction Parameter and the Chain Conformation of Ps-B-Pmma Copolymers. *Macromol.* **2008,** *41*, 4904-4907.
75. Tirumala, V. R.; Daga, V.; Bosse, A. W.; Romang, A.; Ilavsky, J.; Lin, E. K.; Watkins, J. J., Well-Ordered Polymer Melts with 5 Nm Lamellar Domains from Blends of a Disordered Block Copolymer and a Selectively Associating Homopolymer of Low or High Molar Mass. *Macromol.* **2008,** *41*, 7978-7985.
76. Tirumala, V. R.; Romang, A.; Agarwal, S.; Lin, E. K.; Watkins, J. J., Well Ordered Polymer Melts from Blends of Disordered Triblock Copolymer Surfactants and Functional Homopolymers. *Adv. Mater.* **2008,** *20*, 1603-1608.
77. Bosse, A. W.; Douglas, J. F.; Berry, B. C.; Jones, R. L.; Karim, A., Block-Copolymer Ordering with a Spatiotemporally Heterogeneous Mobility. *Phys. Rev. Lett.* **2007,** *99*, 216101-4.
78. Certain equipment, instruments or materials are identified in this paper in order to adequately specify the experimental details. Such identification does not imply recommendation by the National Institute of Standards and Technology nor does it imply the materials are necessarily the best available for the purpose.
79. Savin, D. A.; Pyun, J.; Patterson, G. D.; Kowalewski, T.; Matyjaszewski, K., Synthesis and Characterization of Silica-Graft-Polystyrene Hybrid Nanoparticles: Effect of Constraint on the Glass-Transition Temperature of Spherical Polymer Brushes. *J Polym Sci Pol Phys* **2002,** *40*, 2667-2676.
80. Kim, T. K.; Yang, X. M.; Peters, R. D.; Sohn, B. H.; Nealey, P. F., Chemical Modification of Self-Assembled Monolayers by Exposure to Soft X-Rays in Air. *The Journal of Physical Chemistry B* **2000,** *104*, 7403-7410.
81. Stafford, C. M.; Roskov, K. E.; Epps, T. H.; Fasolka, M. J., Generating Thickness Gradients of Thin Polymer Films Via Flow Coating. *Rev Sci Instrum* **2006,** *77*, 023908.
82. Harrison, C.; Cheng, Z.; Sethuraman, S.; Huse, D. A.; Chaikin, P. M.; Vega, D. A.; Sebastian, J. M.; Register, R. A.; Adamson, D. H., Dynamics of Pattern Coarsening in a Two-Dimensional Smectic System. *Phys. Rev. E* **2002,** *66*, 011706.
83. The data in this manuscript, and in the figures, are presented along with the standard uncertainty involved in the measurement, where the uncertainty represents one standard deviation from the mean.
84. Software made available by Charlie Laub (University of California, Davis).
85. Software made available by Thad Harroun (Brock University).

86. Parratt, L. G., Surface Studies of Solids by Total Reflection of X-Rays. *Phys Rev* **1954,** *95*, 359-369.
87. Plimpton, S., Fast Parallel Algorithms for Short-Range Molecular-Dynamics. *Journal of Computational Physics* **1995,** *117*, 1-19.